Photoelectrocatalytic System as a Reaction Platform for Selective Radical–Radical Coupling

Sunghwan Won,[1] Dongmin Park,[2] Yousung Jung,*[3] Hyunwoo Kim,*[4,5] and Taek Dong Chung*[1,6]

[1]Department of Chemistry, Seoul National University, Seoul 08826, Republic of Korea.

[2]Department of Chemical and Biomolecular Engineering, Korea Advanced Institute of Science and Technology (KAIST), Daejeon 34141, Republic of Korea.

[3]Department of Chemical and Biological Engineering, Institute of Chemical Processes, Seoul National University, Seoul 08826, Republic of Korea.

[4]Department of Chemistry, Pohang University of Science and Technology (POSTECH), Pohang 37679, Republic of Korea.

[5]Institute for Convergence Research and Education in Advanced Technology (I–CREATE), Yonsei University, Seoul 03722, Republic of Korea.

[6]Advanced Institutes of Convergence Technology, Suwon-Si, Gyeonggi-do 16229, Republic of Korea.

Abstract

The selection of electrode material is a critical factor that determines the selectivity of electrochemical organic reactions. However, the fundamental principles governing this relationship are still largely unexplored. Herein, we demonstrate a photoelectrocatalytic (PEC) system as a promising reaction platform for the selective radical–radical coupling reaction owing to the inherent charge-transfer properties of photoelectrocatalysis. As a model reaction, the radical trifluoromethylation of arenes is shown on hematite photoanodes without employing molecular catalysts. The PEC platform exhibited superior mono- to bis-trifluoromethylated product selectivity compared to conventional electrochemical methods utilizing conducting anodes. Electrochemical and density functional theory (DFT) computational studies revealed that controlling the kinetics of anodic oxidation of aromatic substrates is essential for increasing reaction selectivity. Only the PEC configuration could generate sufficiently high-energy charge carriers with controlled kinetics due to the generation of photovoltage and charge-carrier recombination, which are

characteristic features of semiconductor photoelectrodes. This study opens a novel approach towards selective electrochemical organic reactions through understanding the intrinsic physicochemical properties of semiconducting materials.

Introduction

The development of chemoselective synthetic methodology is of utmost importance in organic chemistry. Selectivity is particularly essential for the synthesis of complex organic molecules, as it allows for precise control over multiple reactive sites leading to the efficient and selective construction of desired target molecules. In recent decades, radical-mediated organic transformations have emerged as attractive synthetic strategies enabling the straightforward generation of complex target molecules and overcoming conventional closed-shell reactivity.[1–3] Recent advances by integrating radical intermediates with well-defined homogeneous redox-active catalyst systems[4] or semiconducting particles as photocatalysts[5,6] have been made to achieve the desired chemoselectivity. In particular, heterogeneous electrochemical systems merged with homogeneous transition-metal catalysts pave a new way for the synthesis of target organic molecules. This method takes advantage of the intrinsic strength of electrochemical systems, which enables facile regeneration of heterogeneous catalysts and allows for straightforward scalability, especially when combined with flow systems.[7–9] Typically, the outcomes of the reaction, such as reaction yield, product selectivity, and faradaic efficiency, are closely linked to the choice of electrode materials during operation, although the underlying principles governing this relationship are still largely unexplored.[10]

However, achieving chemoselectivity in radical organic reactions at a heterogeneous interface without the use of homogeneous catalysts remains challenging. The issue lies in the formation of radical intermediates within the electric double layer (EDL) region, a confined space (ca. 1 nm) at the electrode surface, in contrast to homogeneous catalysis. Since highly reactive radical species are produced in this tight space, it is vital to control the radical production kinetics to regulate the local radical concentration and achieve chemoselectivity.[11,12] This is particularly crucial for radical–radical cross-coupling reactions, where balancing the generation kinetics of the two different radical species involved in the reaction is critical for increasing selectivity toward the cross-coupled product.[13–15] Yet, in a typical electrochemical system, matching the radical generation current of the two reactants having different redox potentials is challenging.

On the other hand, the photoelectrocatalytic (PEC) system can be a promising platform for organic reactions involving radical intermediates since the number of charge carriers can be controlled by modulating the illumination intensity. Recently, the use of semiconductor photoelectrodes for the transformation of organic molecules has garnered intensive research interest, owing to its energy-harvesting capability and sustainable features.[9,16–24] Despite the extensive use of photoelectrodes as tools for electron transfer reactions, the impact of the semiconductor itself on the reaction outcome, such as reaction efficiency and product selectivity, remains underexplored.[25] Although regioselective arene C–H amination under the PEC system was previously reported,[21] it is important to note that the selectivity observed in this case was due to the hydrogen bonding network between the reaction intermediate and the solvent, rather than originating from the photoanode itself.

Herein, we describe the inherent advantages of photoelectrodes in radical–radical coupling reactions by demonstrating a mono-selective radical trifluoromethylation of arenes under the photoelectrocatalytic system, which obviates the need of a molecular catalyst (Figure 1). In recent years, the generation of CF_3 radicals by means of single electron transfer (SET) has been shown to be a productive synthetic strategy to access a wide range of trifluoromethylated organic compounds.[26–31] The electrochemical radical trifluoromethylation also has been highlighted in several precedent reports, particularly due to the ability to control the rate of radical formation in the electrochemical method.[32] Recent electrosynthetic techniques such as alternating current electrolysis[33] and electrophotocatalysis[34] were also successfully demonstrated.

Most of the precedent literatures regarding arene radical trifluoromethylation showed modest to low efficiency with electron-rich substrates.[35] Electrochemical trifluoromethylation has recently been developed for highly electron-rich substrates, but the method was not effective for moderately electron-rich and neutral substrates.[36] More importantly, although some prior studies noted the formation of a comparable amount of bis-trifluoromethylated byproducts, limited attention has been devoted to enhancing the selectivity towards mono-substituted products.[33,34,37]

In this study, the newly developed PEC system exhibits good yields and high mono- to bis-trifluoromethylation selectivity, particularly for electron-rich arene substrates compared to electrochemical methods using conducting electrodes such as carbon or fluorine-doped tin oxide (FTO) anodes. Photogenerated holes were capable of oxidizing both arene substrates and the trifluoromethyl (CF_3) radical source, eventually leading to the formation of mono-substituted products through the radical–radical coupling pathway. The exceptional selectivity of the PEC

configuration originates from the charge-transfer characteristics of the photoanode itself, such as charge-carrier recombination and the generation of photovoltage.

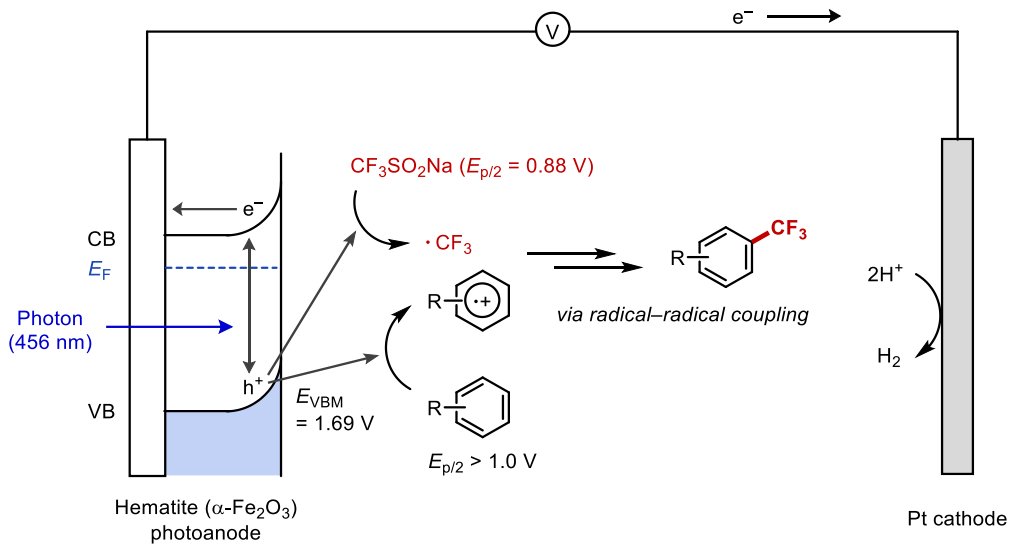

Figure 1. Photoelectrocatalytic trifluoromethylation of arenes. Potential values with respect to Ag/Ag^+.

Results and discussion

Selective mono-trifluoromethylation on the PEC system

We have first examined whether radical trifluoromethylation is a suitable example for demonstrating potential advantages of photoanodes in radical–radical coupling reactions by voltametric studies. Hematite (α-Fe_2O_3) is chosen as a photoanode material due to its fairly positive valence-band maximum (E_{VBM}) and its stable operation in a wide range of organic solvents.[21,38]

Linear sweep voltammograms (LSVs) of sodium trifluoromethanesulfinate (CF_3SO_2Na), a precursor of a CF_3 radical, and aromatic substrates (1,3,5-trimethoxybenzene and anisole) were obtained at a glassy carbon (GC) electrode and a hematite photoanode (Figure 2). At a GC electrode, each compound exhibits distinct onset potentials and current slopes, resulting in significantly different current densities at a certain overpotential (Figure 2a). This is because current–voltage behavior follows Butler-Volmer kinetics under electrolysis conditions, which typically involve high substrate concentrations and forced convection (Figure 2c). Thus, balancing the radical generation currents of the CF_3 radical precursor and the arene substrates is challenging at the conducting anode.

In stark contrast, LSVs obtained at a hematite photoanode under illumination display relatively similar current

densities to each other (Figure 2b). The onset potentials were shifted to more negative values compared to those obtained at a GC electrode, indicating generation of photovoltage at the photoanode.[39] Notably, anisole was directly oxidized by the photoanode at the given potential window, which was not the case with the carbon anode, illustrating the greater oxidation power of hematite due to its sufficiently positive E_{VBM} (Figures 2d, S5). Also, the growth of photocurrents is less rapid compared to the electrochemical system due to charge-carrier recombination.[40] These electrochemical data indicate that a hematite photoanode is more adequate for a radical–radical coupling reaction owing to its ability to "balance" the oxidation current of the two reaction partners (CF_3SO_2Na and an aromatic substrate) and sufficient oxidation power for generating aromatic radical cation.

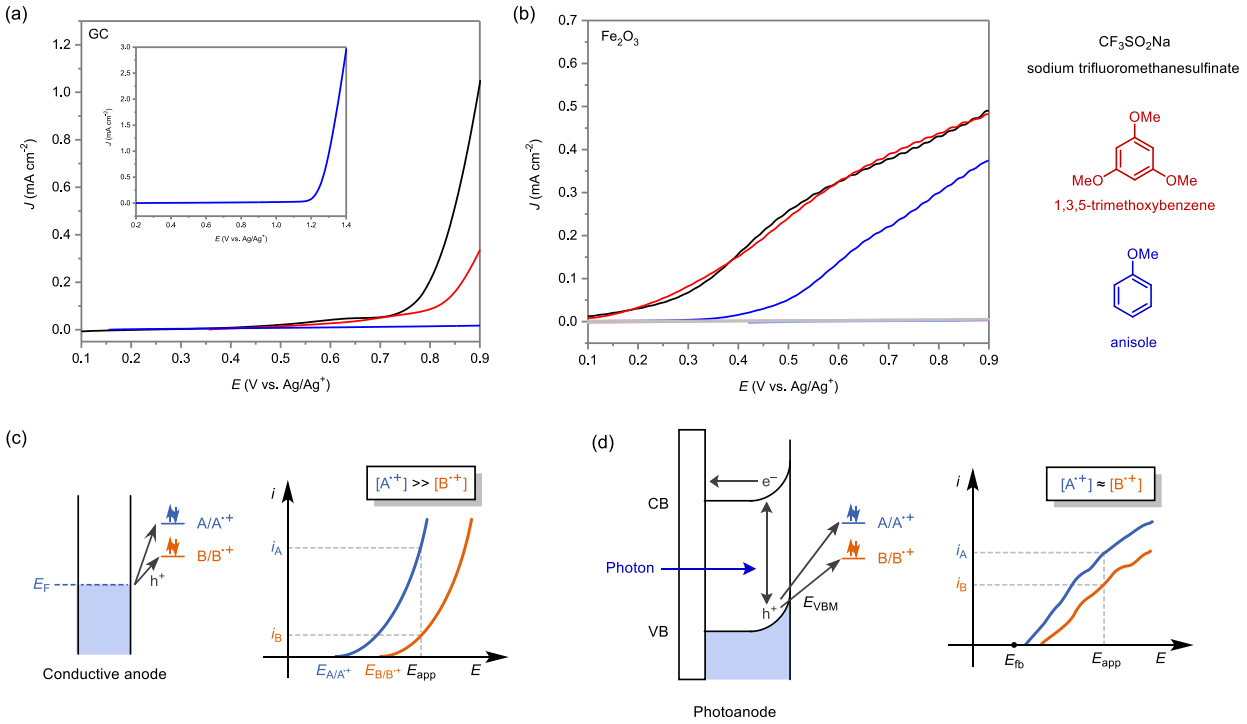

Figure 2. Linear sweep voltammograms (LSVs) of 50 mM substrate solutions in 0.1 M $LiClO_4$ in CH_3CN at (a) a glassy carbon (GC) electrode and (b) a hematite (Fe_2O_3) photoanode under 1 sun illumination (AM 1.5 G; 100 $mW \cdot cm^{-2}$). The pale-colored lines indicate LSVs obtained in the dark. The inset in (a) displays an LSV of anisole at wider potential range. Black = CF_3SO_2Na, red = 1,3,5-trimethoxybenzene, blue = anisole. Scan rate = 50 $mV \cdot s^{-1}$. Schematic representation of charge-transfer pathways and the corresponding *i*–*V* curves in typical (c) electrochemical and (d) PEC systems.

We commenced our investigation by choosing 1,3,5-trimethoxybenzene **1** as our model substrate, hematite as the photoanode and platinum plate as the cathode (Figure 3). The working electrode potential (E_{WE}) was set at 0.8 V, where both the CF_3 radical precursor and **1** could undergo photo-oxidation, and no dark current flowed (Figure 2). After optimization, we observed that the application of both blue light (456 nm) and electric bias was necessary to yield the desired mono-trifluoromethylated product **2** selectively over bis-trifluoromethylated product **3** (Figure 3, entries 1–3). This is because electron–hole pairs are generated through photo-excitation of electrons in the valence band, followed by separation of two charge carriers by an electric field within the space-charge region induced by the applied potential. The optimal conditions employed 2.0 equivalent of CF_3SO_2Na as the radical precursor and $LiClO_4$ as the electrolyte under dimethyl sulfoxide (DMSO) and water as the co-solvent.

The solvent systems other than DMSO/H_2O such as acetonitrile (CH_3CN) were not effective (entry 4). Both reaction yield and product selectivity decreased in the absence of water (entry 5). Furthermore, water was found to be the most efficient proton source compared to other protic co-solvents such as methanol and 1,1,1,3,3,3-hexafluoro-2-propanol (HFIP) (entries 6–7). The choice of electrolyte was also crucial in both reactivity and mono/bis- selectivity (entry 8). When the reaction was carried out under ambient conditions, the mono/bis- selectivity was significantly dropped compared to the standard conditions, while the overall yield was slightly increased (entry 9).

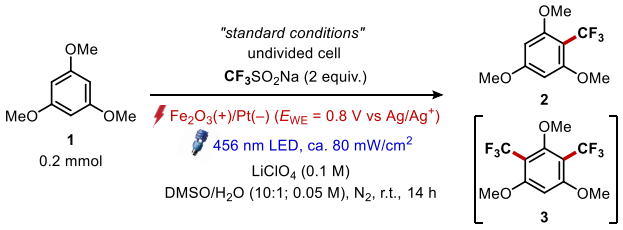

Entry	Variation from "standard conditions"	Yield (%)	Ratio of **2**:**3**
1	none	78	19:1
2	w/o applied voltage	1	-*
3	w/o light	1	-*
4	CH_3CN instead of DMSO	24	>20:1
5	w/o H_2O	61	11:1
6	MeOH instead of H_2O	61	19:1
7	HFIP instead of H_2O	87	5:1
8	$TBAClO_4$ instead of $LiClO_4$	49	4:1
9	under air	88	5:1

* **3** not detected

Figure 3. Reaction parameter optimization. Yields determined by ^{19}F NMR using CF_3CO_2H as an internal standard.

The durability of the electrode is also a crucial factor in electrochemical organic reactions. Often, the electrodes experience surface passivation which is mainly caused by the deposition of polymeric films produced by undefined side reactions of reaction intermediates.[10,41,42] The catalytic activity of a hematite photoanode was retained during five iterative uses (Figure 4a), exhibiting excellent robustness and catalyst-regeneration capability. The surface analysis by using scanning electron microscopy (SEM) and X-ray photoelectron spectroscopy (XPS) further revealed that the morphology, chemical composition, and the band structure of the electrode surface were identical to those of a freshly-prepared photoanode (Figures 4b, c). It is worth mentioning that the carbon-containing polymeric film was not observed, which could potentially lead to passivation of the photoelectrode. The robustness of the hematite surface also highlights its advantage in radical reactions.

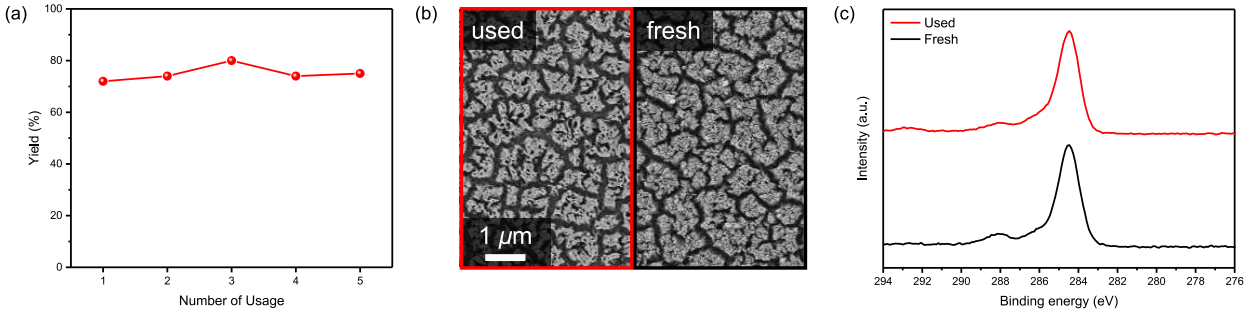

Figure 4. Stability test for iterative usage of the photoanode. (a) Yield of the reaction under the "standard conditions" for five iterative uses. (b) SEM image of a hematite photoanode before and after five iterative uses under the standard reaction conditions. (c) XPS spectra of carbon 1s region before and after five iterative uses.

Next, we employed our optimized reaction conditions to arene substrates with a range of different electronic properties (Figure 5). For the substrates with electron-rich or neutral substituents, moderately high mono- to bis-trifluoromethylation selectivity was observed when using a hematite photoanode. It was notable to see that 1,4-dicyanobenzene showed low reactivity, which cannot be photo-oxidized by the photoanode since its oxidation peak potential is more positive than the E_{VBM} of hematite, ca. 1.7–1.8 V (Figure S5).[38]

For comparative purposes, the reaction was carried out using a carbon-felt anode in a two-electrode configuration, which is one of the most adopted configurations in electrochemical organic synthesis. The cell voltage was chosen within a range where the initial current is closely matched to that of the PEC system (see page S7 in the Supporting

Information for the detailed procedure). Typical cell voltage ranged from 2.6 to 3.2 V, which corresponds to a working electrode potential of 0.6–0.8 V vs. Ag/Ag^+ (Table S1). The semiconductor electrode exhibited notably greater mono/bis-selectivity in contrast to the conducting anode, except in case where 1,4-dicyanobenzene was employed as the substrate (Figure 5).

These results suggest that a semiconductor electrode can selectively produce mono-substituted products when both reactants undergo electrochemical oxidation at the photoanode. This can be attributed to the relatively positive E_{VBM} of hematite and the photovoltage generated within the PEC system, allowing the efficient oxidation of substrates ranging from electron-rich to neutral aromatic compounds, as well as the CF_3 radical source.

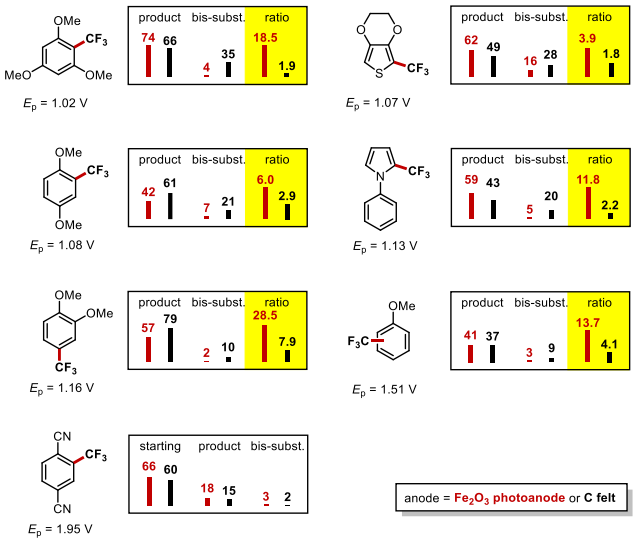

Figure 5. Reaction results when hematite (red) and carbon felt (black) electrodes were used as working electrodes, respectively. Mono- to bis-CF_3 substituted product ratio is presented except for 1,4-dicyanobenzene. First peak potentials of anodic curves (E_p) obtained from 5 mM substrate solutions are reported with respect to an Ag/Ag^+ reference electrode. Bis-subst. = bis-CF_3 substituted product.

DFT computational studies for possible reaction pathways

To explain the superior chemoselectivity of the PEC system, we deliberated the possible reaction pathways of the trifluoromethylation of the aromatic compounds (Figure 6). The CF_3 radical source should first be oxidized to generate a CF_3 radical and consequently, the trifluoromethylated products. The reaction pathways thus bifurcate depending on whether the aromatic substrate is electrochemically oxidized or not (Figure 6a).

When the substrate **1** is oxidized at the (photo)anode surface (Figure 6a-A), the corresponding radical cation $\mathbf{1}^{\bullet+}$ couples with a CF_3 radical, generating the cationic intermediate $\mathbf{[1\text{-}CF_3]}^+$. Deprotonation of $\mathbf{[1\text{-}CF_3]}^+$ gives the mono-substituted product **2**. Thus, the kinetics of the radical–radical coupling pathway will also depend on the oxidation potential of the substrate. On the other hand, the reaction can also be initiated by attack of a CF_3 radical on the aromatic substrate (Figure 6a-B). This radical-attack leads to the formation of the radical intermediate $\mathbf{[1\text{-}CF_3]}^{\bullet}$, followed by the radical-polar crossover at the electrode surface. Rearomatization of the cationic intermediate $\mathbf{[1\text{-}CF_3]}^+$ gives the product **2**.

We anticipate that the radical–radical coupling pathway is dominant on the photoanode since hematite can oxidize the aromatic substrates. On the other hand, the radical-attack pathway is likely to occur when utilizing a carbon anode, since the aromatic compounds were hardly oxidized at the applied potential range, even though the system exhibited a comparable current level (ca. 2 mA) to the PEC configuration (Table S1). The ratio of activation barriers between the mono-substitution step and the bis-trifluoromethylation step will determine the selectivity of the mono-substituted compound **2** over the bis-trifluoromethylated byproduct **3** (the ratio between $\Delta G^{\ddagger}$(1,coup) and $\Delta G^{\ddagger}$(2,coup) for the radical–radical coupling, $\Delta G^{\ddagger}$(1,att) and $\Delta G^{\ddagger}$(2,att) for the radical-attack pathway. See Figure 6 for the abbreviations). Density functional theory (DFT) calculations were performed to obtain kinetic insights of each step (Figure 6b, see page S11 in the Supporting Information for the computational details). The mono-substitution step of the radical–radical coupling pathway occurs without a free-energy barrier since the coupling of two reactive radical species is highly favorable. On the other hand, the activation barrier of the second substitution step is found to be $\Delta G^{\ddagger}$(2,coup) = 6.98 kcal/mol, indicating that the second coupling step is kinetically less favorable than the first one. Also, because the mono-trifluoromethylated compound **2** exhibits more positive oxidation potential compared to the substrate **1**, generating the radical cation $\mathbf{2}^{\bullet+}$ is kinetically slower than $\mathbf{1}^{\bullet+}$ (Figure S7). Consequently, the radical–radical coupling pathway will facilitate kinetically selective formation of the mono-trifluoromethylated product.

On the other hand, relatively similar activation barriers of $\Delta G^{\ddagger}$(1,att) = 13.70 kcal/mol and $\Delta G^{\ddagger}$(2,att)=14.47 kcal/mol were obtained for the radical-attack pathway. This result implies that achieving mono-to-bis trifluoromethylation selectivity is less probable under mild overpotential conditions insufficient to oxidize the aromatic compounds. It is noteworthy that a CF_3 radical is less likely to attack **1** or **2** instead of $\mathbf{1}^{\bullet+}$ when the oxidation potential of a hole is sufficiently high, since $\Delta G^{\ddagger}$(1,att) and $\Delta G^{\ddagger}$(2,att) are much greater than $\Delta G^{\ddagger}$(1,coup). The energy

profile demonstrated in Figure 6 represents the result at 1.8 V. However, the activation barriers of the radical-attack pathway at 0.8 V were identical to those obtained at 1.8 V, as the change in electrode potential only affects the free energy of the electron-transfer steps (Figure S10).

Thus, the present computational study suggests that sufficiently positive valence band position of hematite facilitates direct electrochemical oxidation of the aromatic compounds, eventually leading to a selective production of mono-substituted product through radical–radical coupling. This explanation is consistent with the experimental result that both the PEC system and the carbon anode-based electrochemical setup exhibited identical reaction result with the highly electron-deficient substrate that cannot be directly oxidized by a hematite photoanode (Figure 5).

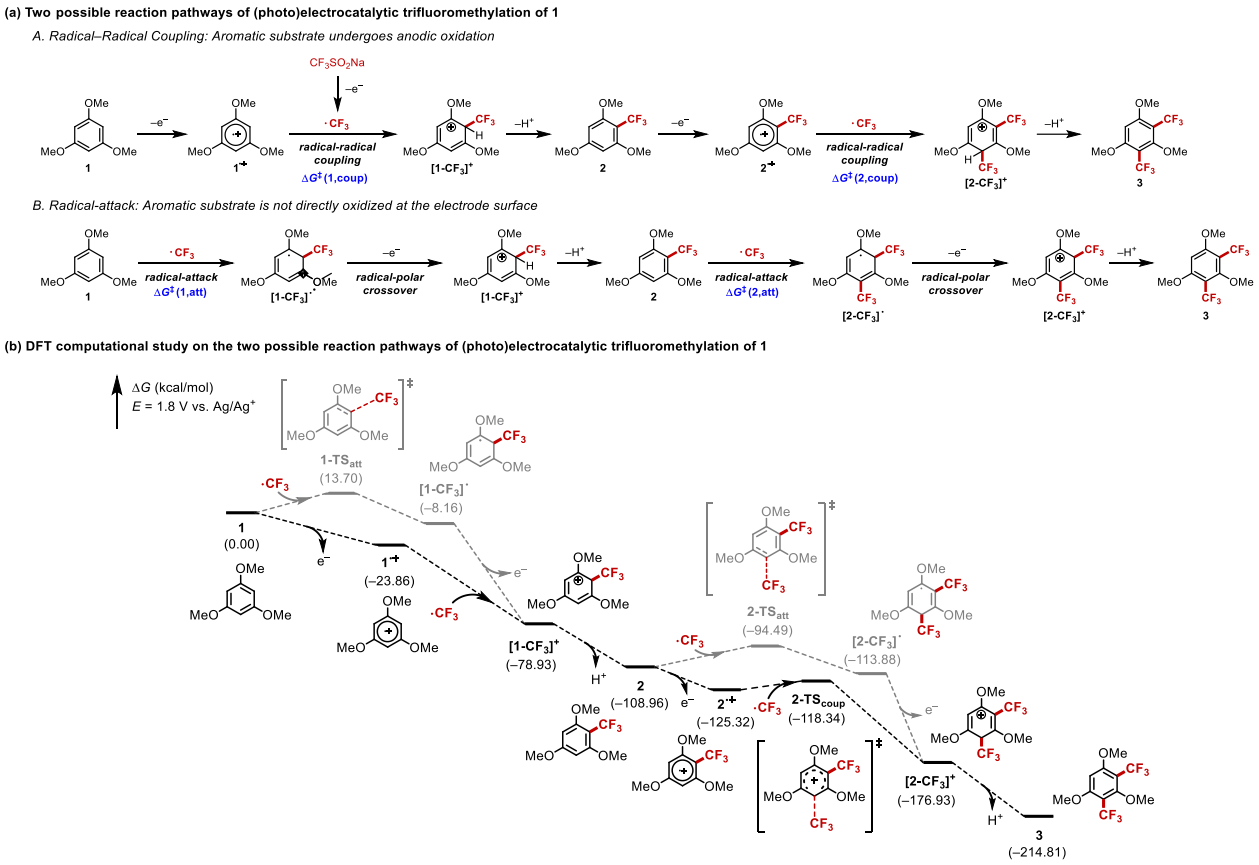

Figure 6. (a) Two possible reaction pathways of (photo)electrocatalytic (bis-)trifluoromethylation of **1**. (b) DFT computational study on the two possible reaction pathways at E = 1.8 V vs. Ag/Ag^+. Pathway drawn in black = radical–radical coupling, grey = radical-attack.

Inherent advantages of the PEC configuration in selective radical reactions

Given that direct oxidation of the substrate may enhance the selectivity of the mono-substituted product, a series of electrochemical systems utilizing different electrode materials was employed for the trifluoromethylation of 1 to explore whether sufficient overpotential can improve the selectivity of electrochemical configurations (Figure 7).

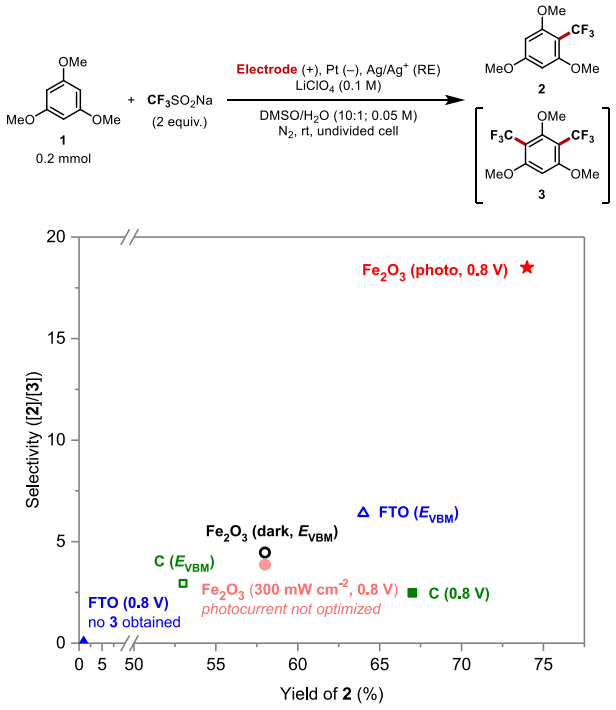

Figure 7. Reaction yield and selectivity depending on electrode material and applied voltage. E_{VBM} corresponds to the valence band edge of hematite, 1.8 V vs. Ag/Ag^+.

First, the reaction was conducted with a hematite electrode in the dark at 1.8 V, which approximately corresponds to the E_{VBM}, to dictate the direct electrochemical oxidation of the substrate without light irradiation (black open circle). Both the yield and mono/bis-selectivity were reduced, implying that the PEC reaction condition (red star) outperforms its purely electrochemical counterpart. It is known that electrochemical oxidation is not possible on the hematite surface in the absence of light due to its nature as an n-type semiconducting material.[43] Consequently, the oxidation of organic molecules is expected to take place at the pinholes of the underlying conductive substrate, FTO.[44,45] Comparable yields and product ratios to the dark condition were observed when employing a bare FTO electrode as the anode (blue open triangle), suggesting that the hematite layer does not exhibit catalytic activity under dark

conditions. Hence, the reaction selectivity of the PEC system should be explained by the charge transfer characteristics under illumination.

Conversely, no reaction took place at FTO at 0.8 V (blue filled triangle), which corresponds to the operating potential of the PEC system, as it is a relatively inert electrode material that demands a greater overpotential to facilitate the identical electron transfer reaction (Figure S8). The reaction was also conducted using a carbon anode at 0.8 V within a three-electrode system. Although the initial current level was almost identical to that of the PEC system, the inferior mono- to bis-trifluoromethylation selectivity was observed (green filled square), consistent with the computational result.

When a potential of 1.8 V was applied to a carbon anode for the direct electrochemical oxidation of the substrate, it resulted in a slight increase in product selectivity but a decrease in the overall yield (green open square). The decrease in overall reaction yield can be attributed to the significant increase in current resulting from the application of high voltage. Owing to the elevated current density, a considerable amount of radical intermediates is generated in close proximity to the electrode surface, rendering the radical reaction uncontrollable and ultimately leading to a reduction in overall yield of the cross-coupled product.[11,12] A similar reactivity pattern was observed with the semiconductor electrode. When the initial current was increased by the strong irradiation (ca. 300 $mW \cdot cm^{-2}$) while maintaining a constant overpotential, the product yield was deteriorated from 74% to 58% (pale red, filled circle). The elevated current density also deteriorated the product selectivity from the standard PEC reaction conditions, possibly because excessive charge carriers caused the oxidation of the mono-substituted product **2**, thereby facilitating the second trifluoromethylation step.

Therefore, we have concluded that the reaction yield and product selectivity should be compromised at an electrochemical system utilizing a conducting electrode. At a low overpotential, the radical–radical coupling reaction cannot occur, resulting in relatively unselective behavior. At a high overpotential, even though reaction selectivity slightly increases due to radical–radical coupling, overall yield decreases because of high current density and generation of excess radical species. Since current and overpotential are coupled at a metal-like electrode and cannot be independently optimized, additional strategies such as surface modification with electron-transfer mediators and/or incorporation of homogeneous catalysts are needed to enhance the selectivity of electrochemical systems.[46]

On the other hand, overpotential and photocurrent density can be independently tuned when using photoelectrodes

because the number of photogenerated charge carriers is not only a function of overpotential but also depends on the illumination intensity. This characteristic feature of semiconductor photoelectrodes enables independent optimization of photocurrents under constant overpotential, while securing sufficient redox power by carefully selecting semiconducting material with a suitable band-edge alignment.

Numerous applications can stem from the intrinsic physicochemical properties of semiconductor photoelectrodes highlighted in this study. For instance, introducing various surface defects can help regulate the spatial distribution of 'hole-emitting' sites, where radical intermediates are generated.[47] Since the allocation of catalytic sites significantly affects the efficiency of radical coupling reactions,[48] appropriate surface treatment will maximize the benefits of PEC systems in these reactions.

Several characteristic features of a photoelectrode that have not been experimentally examined in this research may also affect the selectivity of reactions. For example, the presence of surface states is a representative distinctive feature of photoelectrodes compared to metal-like electrodes.[45,49,50] However, their role in the transformation of organic molecules has not been thoroughly investigated to date. The presence of native surface states may result in photogenerated holes having different oxidation potentials at the electrode surface, just before their transfer into the solution phase (Figure S9). This, in turn, could reduce the difference between the effective overpotential for each oxidation reaction (η_1 and η_2 in Figure S9), consequently decreasing the disparity in the two oxidation currents.

In summary, we have explored the impact of distinct charge-transfer characteristics of a semiconductor photoelectrode on the selectivity of radical reaction by demonstrating PEC trifluoromethylation of aromatic compounds as a model reaction. Since a PEC system is capable of controlled release of highly reactive minority charge carriers as well as balancing the radical generation currents between the two radical precursors, a selective radical–radical coupling reaction was successively achieved without help of a transition-metal-based homogeneous catalyst. Considering that the choice of electrode material significantly influences reaction outcomes, studying the impact of the charge-transfer characteristics of photoelectrodes on the reaction result will facilitate the development of more efficient PEC organic synthesis methods, as well as understanding mechanistic features.

Methods

Preparation of the photoanode

Hematite photoelectrodes were synthesized according to the previously reported procedure.[51,52] Briefly, cleaned fluorine-doped tin oxide (FTO, Solaronix, Switzerland) glass was soaked in a precursor solution containing 0.15 M $FeCl_3$ and 1.0 M $NaNO_3$, and enclosed with stainless steel autoclave. The temperature of the system was raised to 95 °C and kept for 4 hours to form β-FeOOH film on the FTO substrate. After cooled at 4 °C for 45 minutes, the electrodes were sonicated for 3 minutes to remove poorly adsorbed particles. The substrates were then annealed at 550 °C for 2 hours to convert the as-deposited β-FeOOH film into hematite (α-Fe_2O_3) nanowire. Then, the hematite electrodes were additionally annealed at 800 °C for 20 minutes to improve their PEC activity.

General Procedure for Photoelectrocatalytic Trifluoromethylation of Arenes

Electrolysis experiments were conducted using an MPG-2 multi-potentiostat (Biologic). Kessil PR160 blue LED (λ = 456 nm) is used as a light source. An oven-dried, 10 mL two-neck glass tube was equipped with a magnetic stir bar, a rubber septum, a threaded Teflon cap fitted with electrical feed-throughs, a hematite photoanode (1.0×1.0 cm^2, connected to the electrical feedthrough via a 9 cm in length, 2 mm in diameter graphite rod), a platinum mesh cathode (0.5×1.0 cm^2), and an Ag/Ag^+ reference electrode. To this reaction vessel, $LiClO_4$ (42.5 mg, 0.4 mmol), an arene subsrate (0.2 mmol, 1.0 equiv.), and CF_3SO_2Na (62.4 mg, 0.4 mmol, 2 equiv.) were added. The cell was sealed and purged with a nitrogen-filled balloon for 15 minutes. Before initiating the photoelectrocatalytic reaction, a cyclic voltammogram was obtained in the dark to determine the potential range where dark current does not flow. Typical potential-range limit was 0.6–0.8 V, where the initial current was approximately 2 mA. The photoelectrochemical reaction was conducted under illumination with a blue LED (distance ~ 5 cm) at room temperature for 14–18 hours. The reaction mixture was then filtered by silica or Celite and concentrated under reduced pressure. The residue was subjected to flash column chromatography on silica gel (eluted with hexane/ethyl acetate) to yield the desired product.

Procedures for Voltammetric Studies

(Photo)electrochemical experiments were conducted using a Gamry Reference 600 potentiostat (Gamry Instruments). A glassy carbon (GC) rod electrode (d = 4 mm) or an FTO glass was used as a working electrode. A platinum wire was used as a counter electrode. Ag/Ag^+ reference electrode was used as a reference electrode. For an FTO glass, a homemade Teflon electrochemical cell was used, and electrode area was defined by a super-viton P6 O-

ring (inner diameter = 5.8 mm; Anyseal, Korea). Scan rate is 50 mV/s, unless otherwise noted.

Computational Details

Density functional theory (DFT) calculations were conducted using Q-Chem 4.4 program[53] to obtain optimized structures and energies of each reactant, product, transition state, and intermediate species. The range-separated ωB97X-D3 hybrid functional[54] with the 6-31G* basis set[55] was used for geometry optimizations and vibrational frequency analysis. Solvation effects were considered using the polarizable continuum model (PCM) as implemented in Q-Chem,[56] with a dielectric constant of 46.7, corresponding to that of DMSO. To obtain the Gibbs free energy, thermal corrections were applied to the single point electron energy obtained on optimized structures with the same functional but with the larger def2-TZVP basis set.[57]

To account for the potential effects, the computational hydrogen electrode method was applied as in the previously reported case.[58] In the computational hydrogen electrode method, the chemical potential of the electron is referenced to the standard hydrogen electrode (SHE) and the applied potential relative to the SHE.

Spin-polarized DFT calculations for surface adsorption were performed using the Vienna Ab Initio Simulation Package (VASP) 6.4.2. The exchange correlation energy effects were implemented with the generalized gradient approximation (GGA) using the Perdew-Burke-Ernzerhof (PBE) functional.[59] A plane-wave basis was used with a cut-off energy of 400 eV, and the projector augmented wave method was used to describe the interactions of the atomic core regions and electrons.[60,61] All geometry optimizations were performed until the atomic-forces were minimized to less than 0.05 eV/Å.

Data availability

All data is available in the main text or Supplementary Information.

References

1. Parsaee, F. *et al.* Radical philicity and its role in selective organic transformations. *Nat. Rev. Chem.* **5**, 486–499 (2021).

2. Yan, M., Lo, J. C., Edwards, J. T. & Baran, P. S. Radicals: Reactive Intermediates with Translational Potential.

J. Am. Chem. Soc. **138**, 12692–12714 (2016).

3. Zhang, N., Samanta, S. R., Rosen, B. M. & Percec, V. Single electron transfer in radical ion and radical-mediated organic, materials and polymer synthesis. *Chem. Rev.* **114**, 5848–5958 (2014).
4. Mahmudov, K. T. & Pombeiro, A. J. L. Control of Selectivity in Homogeneous Catalysis through Noncovalent Interactions. *Chem. Eur. J.* **29**, e202203861 (2023).
5. Kisch, H. Semiconductor Photocatalysis for Chemoselective Radical Coupling Reactions. *Acc. Chem. Res.* **50**, 1002–1010 (2017).
6. Horner, G. *et al.* Semiconductor Type A Photocatalysis: Role of Substrate of Photoreactive Surface Sites in Zinc Sulfide Catalyzed C-C Coupling Reactions. *Chem. Eur. J.* **5**, 208–217 (1999).
7. Noël, T., Cao, Y. & Laudadio, G. The Fundamentals behind the Use of Flow Reactors in Electrochemistry. *Acc. Chem. Res.* **52**, 2858–2869 (2019).
8. Chen, L. *et al.* Electrochemical Cyclobutane Synthesis in Flow: Scale-Up of a Promising Melt-Castable Energetic Intermediate. *Org. Process Res. Dev.* **25**, 2639–2645 (2021).
9. Chen, Y. *et al.* Scalable decarboxylative trifluoromethylation by ion-shielding heterogeneous photoelectrocatalysis. *Science* **384**, 670–676 (2024).
10. Heard, D. M. & Lennox, A. J. J. Electrode Materials in Modern Organic Electrochemistry. *Angew. Chem. Int. Ed.* **59**, 18866–18884 (2020).
11. Huang, H. *et al.* A Liquid-Liquid-Solid System to Manipulate the Cascade Reaction for Highly Selective Electrosynthesis of Aldehyde. *Angew. Chem. Int. Ed.* **62**, e202216321 (2023).
12. Wuttig, A. & Toste, F. D. The interface is a tunable dimension in electricity-driven organic synthesis. *Nat. Sci.* **1**, e20210036 (2021).
13. Claridge, R. F. C. & Fischer, H. Self-Termination and Electronic Spectra of Substituted Benzyl Radicals in Solution. *J. Phys. Chem.* **87**, 1960–1967 (1983).
14. Wang, S., Tang, S. & Lei, A. Tuning radical reactivity for selective radical/radical cross-coupling. *Sci. Bull.* **63**, 1006–1009 (2018).
15. Mo, Y. *et al.* Microfluidic electrochemistry for single-electron transfer redox-neutral reactions. *Science* **368**, 1352–1357 (2020).

16. Cha, H. G. & Choi, K. S. Combined biomass valorization and hydrogen production in a photoelectrochemical cell. *Nat. Chem.* **7**, 328–333 (2015).

17. Li, T. *et al.* Photoelectrochemical oxidation of organic substrates in organic media. *Nat. Commun.* **8**, 390 (2017).

18. Li, Z. *et al.* Photoelectrocatalytic C–H halogenation over an oxygen vacancy-rich TiO_2 photoanode. *Nat. Commun.* **12**, 6698 (2021).

19. Zhao, Y. *et al.* α-Fe_2O_3 as a versatile and efficient oxygen atom transfer catalyst in combination with H_2O as the oxygen source. *Nat. Catal.* **4**, 684–691 (2021).

20. Tateno, H., Iguchi, S., Miseki, Y. & Sayama, K. Photo-Electrochemical C−H Bond Activation of Cyclohexane Using a WO_3 Photoanode and Visible Light. *Angew. Chem. Int. Ed.* **57**, 11238–11241 (2018).

21. Zhang, L. *et al.* Photoelectrocatalytic arene C–H amination. *Nat. Catal.* **2**, 366–373 (2019).

22. Liu, X. *et al.* Bromide-Mediated Photoelectrochemical Epoxidation of Alkenes Using Water as an Oxygen Source with Conversion Efficiency and Selectivity up to 100%. *J. Am. Chem. Soc.* **144**, 19770–19777 (2022).

23. Wu, L. *et al.* Competitive Non-Radical Nucleophilic Attack Pathways for NH_3 Oxidation and H_2O Oxidation on Hematite Photoanodes. *Angew. Chem. Int. Ed.* e202214580 (2022).

24. Wang, J. *et al.* Al_2O_3-coated $BiVO_4$ Photoanodes for Photoelectrocatalytic Regioselective C–H Activation of Aromatic Amines. *Angew. Chem. Int. Ed.* e202315478 (2023).

25. Beranek, R. Selectivity of Chemical Conversions: Do Light-Driven Photoelectrocatalytic Processes Hold Special Promise? *Angew. Chem. Int. Ed.* **58**, 16724–16729 (2019).

26. Ji, Y. *et al.* Innate C-H trifluoromethylation of heterocycles. *Proc. Natl. Acad. Sci. U. S. A.* **108**, 14411–14415 (2011).

27. Lu, X. *et al.* Regioselective C–H Trifluoromethylation of Aromatic Compounds by Inclusion in Cyclodextrins. *Org. Lett.* **23**, 4327–4331 (2021).

28. Ye, Y., Lee, S. H. & Sanford, M. S. Silver-mediated trifluoromethylation of arenes using $TMSCF_3$. *Org. Lett.* **13**, 5464–5467 (2011).

29. Natte, K. *et al.* Palladium-Catalyzed Trifluoromethylation of (Hetero)Arenes with CF_3Br. *Angew. Chem. Int. Ed.* **55**, 2782–2786 (2016).

30. Meucci, E. A. *et al.* Nickel(IV)-Catalyzed C-H Trifluoromethylation of (Hetero)arenes. *J. Am. Chem. Soc.* **141**, 12872–12879 (2019).

31. Studer, A. A 'renaissance' in radical trifluoromethylation. *Angew. Chem. Int. Ed.* **51**, 8950–8958 (2012).

32. O-Brien, A. G. *et al.* Radical C-H functionalization of heteroarenes under electrochemical control. *Angew. Chem. Int. Ed.* **53**, 11868–11871 (2014).

33. Rodrigo, S. *et al.* Alternating current electrolysis for organic electrosynthesis: Trifluoromethylation of (hetero)arenes. *Org. Lett.* **22**, 6719–6723 (2020).

34. Qiu, Y., Scheremetjew, A., Finger, L. H. & Ackermann, L. Electrophotocatalytic Undirected C−H Trifluoromethylations of (Het)Arenes. *Chem. Eur. J.* **26**, 3241–3246 (2020).

35. Dou, G. Y., Jiang, Y. Y., Xu, K. & Zeng, C. C. Electrochemical Minisci-type trifluoromethylation of electron-deficient heterocycles mediated by bromide ions. *Org. Chem. Front.* **6**, 2392–2397 (2019).

36. Deng, Y. *et al.* External-Oxidant-Free Electrochemical Oxidative Trifluoromethylation of Arenes Using CF_3SO_2Na as the CF_3 Source. *Chinese J. Chem.* **37**, 817–820 (2019).

37. Struwe, J. & Ackermann, L. Photoelectro-Catalyzed Undirected C–H Trifluoromethylation of Arenes: Catalyst Evaluation and Scope. *Faraday Discuss.* **247**, 79–86 (2023).

38. Sivula, K., Le Formal, F. & Grätzel, M. Solar Water Splitting Progress Using Hematite Photoelectrodes. *ChemSusChem* **4**, 432–449 (2011).

39. Mayer, M. T. Photovoltage at semiconductor–electrolyte junctions. *Curr. Opin. Electrochem.* **2**, 104–110 (2017).

40. Corby, S., Rao, R. R., Steier, L. & Durrant, J. R. The kinetics of metal oxide photoanodes from charge generation to catalysis. *Nat. Rev. Mater.* **6**, 1136–1155 (2021).

41. Ferreira, M., Varela, H., Torresi, R. M. & Tremiliosi-Filho, G. Electrode passivation caused by polymerization of different phenolic compounds. *Electrochim. Acta* **52**, 434–442 (2006).

42. Gattrell, M. & Kirk, D. W. A Study of Electrode Passivation during Aqueous Phenol Electrolysis. *J. Electrochem. Soc.* **140**, 903–911 (1993).

43. Eisenberg, D., Ahn, H. S. & Bard, A. J. Enhanced photoelectrochemical water oxidation on bismuth vanadate by electrodeposition of amorphous titanium dioxide. *J. Am. Chem. Soc.* **136**, 14011–14014 (2014).

44. Shadabipour, P. & Hamann, T. W. Interface passivation to overcome shunting in semiconductor-catalyst junctions. *Chem. Commun.* **56**, 2570–2573 (2020).

45. Seo, D., Won, S., Kim, J. T. & Chung, T. D. Adopting Back Reduction Current as an Additional Output Signal for Achieving Photoelectrochemical Differentiated Detection. *Anal. Chem.* **94**, 2063–2071 (2022).

46. Francke, R. & Little, R. D. Redox catalysis in organic electrosynthesis: Basic principles and recent developments. *Chem. Soc. Rev.* **43**, 2492–2521 (2014).

47. Chen, R., Fan, F. & Li, C. Unraveling Charge-Separation Mechanisms in Photocatalyst Particles by Spatially Resolved Surface Photovoltage Techniques. *Angew. Chem. Int. Ed.* **61**, e202117567 (2022).

48. Yu, J. *et al.* Electroreductive coupling of benzaldehyde by balancing the formation and dimerization of the ketyl intermediate. *Nat. Commun.* **13**, 7909 (2022).

49. Peter, L. M. Dynamic Aspects of Semiconductor Photoelectrochemistry. *Chem. Rev.* **90**, 753–769 (1990).

50. Peter, L. M., Wijayantha, K. G. U. & Tahir, A. A. Kinetics of light-driven oxygen evolution at α-Fe_2O_3 electrodes. *Faraday Discuss.* **155**, 309–322 (2012).

51. Ling, Y., Wang, G., Wheeler, D. A., Zhang, J. Z. & Li, Y. Sn-doped hematite nanostructures for photoelectrochemical water splitting. *Nano Lett.* **11**, 2119–2125 (2011).

52. Vayssieres, L., Beermann, N., Lindquist, S. E. & Hagfeldt, A. Controlled aqueous chemical growth of oriented three-dimensional crystalline nanorod arrays: Application to iron(III) oxides. *Chem. Mater.* **13**, 233–235 (2001).

53. Shao, Y. *et al.* Advances in molecular quantum chemistry contained in the Q-Chem 4 program package. *Mol. Phys.* **113**, 184–215 (2015).

54. Lin, Y. S., Li, G. De, Mao, S. P. & Chai, J. Da. Long-range corrected hybrid density functionals with improved dispersion corrections. *J. Chem. Theory Comput.* **9**, 263–272 (2013).

55. Hariharan, P. C. & Pople, J. A. The Influence of Polarization Functions on Molecular Orbital Hydrogenation Energies. *Theor. chim. Acta* **28**, 213–222 (1973).

56. Lange, A. W. & Herbert, J. M. Polarizable continuum reaction-field solvation models affording smooth potential energy surfaces. *J. Phys. Chem. Lett.* **1**, 556–561 (2010).

57. Weigend, F. & Ahlrichs, R. Balanced basis sets of split valence, triple zeta valence and quadruple zeta valence

quality for H to Rn: Design and assessment of accuracy. *Phys. Chem. Chem. Phys.* **7**, 3297–3305 (2005).

58. Huang, Y., Nielsen, R. J., Goddard, W. A. & Soriaga, M. P. The Reaction Mechanism with Free Energy Barriers for Electrochemical Dihydrogen Evolution on MoS_2. *J. Am. Chem. Soc.* **137**, 6692–6698 (2015).

59. Perdew, J. P., Burke, K. & Ernzerhof, M. Generalized gradient approximation made simple. *Phys. Rev. Lett.* **77**, 3865–3868 (1996).

60. Blöchl, P. E. Projector augmented-wave method. *Phys. Rev. B* **50**, 17953–17979 (1994).

61. Kresse, G. & Furthemuller, J. Efficient iterative schemes for ab initio total-energy calculations using a plane-wave basis set. *Phys. Rev. B* **54**, 11169–11186 (1996).

Acknowledgements

This work was supported by the National Research Foundation of Korea (NRF) grant funded by the Korea government (MSIT) (No. 2021R1A5A1030054). This work was supported by the National Research Foundation of Korea (NRF) grant funded by the Korea government (MSIT) (No. 2022R1A2C3004327). This work was supported by the National Research Foundation of Korea (NRF) grant funded by the Korea government (MSIT) (No. 2021R1C1C1004605). S.W. acknowledges Dr. Su Yong Go for his assistance and advice on the product purification. S.W. also thanks Mr. Jinyeong Park, Mr. Donghwi Na, Ms. Ji Yong Kim, Mr. Sung Il Kim, and Dr. Jeonguk Kweon for their technical support and fruitful discussion.

Author contributions

S.W., H.K., and T.D.C. conceived the initial idea.; S.W. performed most of the experiments.; D.P. performed the DFT analysis under the supervision of Y.J.; H.K. and T.D.C. supervised the overall project.; S.W., H.K., and T.D.C. wrote the initial draft.; All the authors revised the paper and have given approval to the final version of the manuscript.

Competing interests

The authors declare no competing interest.